The Astrophysical Journal, 727:31 (13pp), 2011 January 20 doi:10.1088/0004-637X/727/1/31

X-RAY PROPERTIES OF NARROW-LINE SEYFERT 1 GALAXIES WITH VERY SMALL BROADLINE WIDTHS

Y. L. Ai[1,4], W. Yuan[2,4], H. Y. Zhou[3], T. G. Wang[3], and S. H. Zhang[3]
[1] National Astronomical Observatories/Yunnan Observatory, Chinese Academy of Sciences, Kunming, Yunnan, P.O. Box 110, China; ayl@ynao.ac.cn
[2] National Astronomical Observatories, Chinese Academy of Sciences, Beijing 100012, China; wmy@nao.cas.cn
[3] Key Laboratory for Research in Galaxies and Cosmology, Center for Astrophysics, University of Science and Technology of China, Hefei, Anhui, China
Received 2009 November 27; accepted 2010 November 12; published 2010 December 29

ABSTRACT

Narrow-line Seyfert 1 galaxies (NLS1s) with very small broadline widths (say, FWHM(Hβ) $\lesssim$1200 km s^{-1}) represent the extreme type of Seyfert 1 galaxies that have small black hole masses ($M_{\rm BH}$) and/or high Eddington ratios ($L/L_{\rm Edd}$). Here, we study the X-ray properties of a homogeneously and optically selected sample of 13 such objects, termed as very narrow line Seyfert 1 galaxies, using archival *XMM-Newton* data. It is found that the Fe Kα emission line is at most weak in these objects. A soft X-ray excess is ubiquitous, with the thermal temperatures falling within a strict range of 0.1–0.2 keV. Our result highlights the puzzling independence of the thermal temperature by extending the relations to even smaller FWHM(Hβ), i.e., smaller $M_{\rm BH}$ ($\sim10^6\ M_\odot$) and/or higher $L/L_{\rm Edd}$. The excess emission can be modeled by a range of viable models, though the disk reflection and Comptonization models generally give somewhat better fits over the smeared absorption and the *p*-free models. At the Eddington ratios around unity and above, the X-ray spectral slopes in the 2–10 keV band are systematically flatter than the predictions of the relationship with $L/L_{\rm Edd}$ suggested previously. Short timescale (1–2 hr) X-ray variability is common, which, together with the variability amplitude computed for some of the objects, is supportive of the scenario that NLS1s are indeed active galactic nuclei with relatively small $M_{\rm BH}$.

Key words: galaxies: active – galaxies: Seyfert – X-rays: galaxies

Online-only material: color figures

1. INTRODUCTION

Type 1 active galactic nuclei (AGNs) are characterized by prominent broad emission lines in their optical/UV spectra. The lower end of the linewidths is mostly populated by the so-called narrow-line Seyfert 1 galaxies (NLS1s), defined as having the broad hydrogen Balmer lines narrower than $\sim$2000 km s^{-1} in full width at half-maximum (FWHM) and the relatively weak [O III] lines (Osterbrock & Pogge 1985; Goodrich 1989). NLS1s show some extreme properties among AGNs (see Komossa 2008 for a recent review). Previous studies have revealed a set of correlations among AGN optical emission lines and X-ray properties—the so-called eigenvector 1 (EV1) correlations (Boroson & Green 1992), which are believed to be driven by the Eddington ratio ($L/L_{\rm Edd}$). A narrow Hβ line is generally associated with strong optical Fe II and weak [O III] emission (Goodrich 1989; Véron-Cetty et al. 2001), a steep soft X-ray spectral slope (Boller et al. 1996; Wang et al. 1996), and fast and large amplitude X-ray variability (Leighly 1999; Grupe 2004). However, these correlations were found based on AGNs with FWHM(Hβ) mostly broader than $\sim$1000 km s^{-1}, below which only a small number of objects were known by then. One would expect naively, based on the EV1 correlations, that NLS1s with very small widths (say, FWHM $\lesssim$ 1000 km s^{-1}) would show even extreme properties in X-ray, i.e., even steeper soft X-ray slopes and even faster and larger amplitude variability. We refer to such AGNs as very narrow line Seyfert 1 galaxies (VNLS1s) hereafter in this paper.

It has been recently found that the gas motion in the broadline region (BLR) is virialized (Peterson & Wandel 2000; Onken & Peterson 2002) and that the BLR size scales with optical luminosity with an index of roughly 0.5 (Kaspi et al. 2005; Bentz et al. 2006). A combination of these properties naturally links FWHM(Hβ) with black hole mass $M_{\rm BH}$ and $L/L_{\rm Edd}$ in a way as FWHM^4 $\sim M_{\rm BH}(L/L_{\rm Edd})^{-1}$ (McHardy et al. 2006). Therefore, a narrower FWHM(Hβ) indicates a larger $(L/L_{\rm Edd})/M_{\rm BH}$ ratio, provided that the inclination is not a dominating effect. This is what NLS1s are commonly thought to be, as argued extensively in the literature (e.g., Mineshige et al. 2000; Peterson et al. 2000; Sulentic et al. 2000), and should be even more extreme for VNLS1s as expected.

As such, the X-ray properties of these extreme black hole accreting systems are of particular interest, in light of the following considerations. First, VNLS1s are well suited for investigating the soft X-ray excess emission commonly detected in Seyfert 1 galaxies and quasars, whose origins remain controversial. One motivation is to attempt to link the soft X-ray excess with the blackbody emission from accretion disks, whose maximum temperature would be the highest among AGNs currently known (since $T_{\rm max} \propto[(L/L_{\rm Edd})/M_{\rm BH}]^{1/4} \propto ({\rm FWHM})^{-1}$), and might be detectable with the current X-ray satellites. Interestingly, this attempt was successful in at least one AGN, RX J1633+4718, that is also a VNLS1 (FWHM(Hβ) $\sim$ 900 km s^{-1}) but radio loud, as recently discovered by Yuan et al. (2010), though similar cases are extremely rare. Alternatively, the observed soft X-ray excess can be mimicked by relativistically blurred line emission of the reflection component from a highly ionized inner disk, which may be dominant in high $L/L_{\rm Edd}$ systems (Fabian et al. 2002). Second, there were suggestions that NLS1s resemble the fastest accreting states ("high" and "very high" states) of X-ray binaries, in both the X-ray spectra (e.g., Pounds et al. 1995; Middleton et al. 2007) and X-ray quasi-periodic oscillations (Gierliński et al. 2008), and thus VNLS1s are more suitable for studying such an analogy. Third, the X-ray spectral and temporal

[4] Also at Key Laboratory for the Structure and Evolution of Celestial Objects, Chinese Academy of Sciences, Kunming, China.

Table 1
Basic Parameters of the Sample Objects

No. (1)	Name (2)	SDSS Name (3)	z (4)	$\log\lambda L_{\lambda 5100}$ (5)	FWHM(Hβ) (6)	FWHM(Hα) (7)	$F(\mathrm{H}\alpha^{\mathrm{bc}})$ (8)	R_{4570} (9)	$\log M_{\mathrm{BH}}$ (10)	$\log L_{\mathrm{bol}}/L_{\mathrm{Edd}}$ (11)
1	J0107+1408	J010712.0+140845	0.076	42.96	787 ± 31	709 ± 12	1500 ± 12	0.35 ± 0.05	5.87	−0.13
2	J0740+3118	J074020.2+311841	0.295	44.20	1135 ± 28	1090 ± 17	2121 ± 24	0.92 ± 0.05	6.90	0.073
3	J0922+5120	J092247.0+512038	0.159	44.01	1132 ± 27	1002 ± 13	3058 ± 23	1.37 ± 0.04	6.63	0.145
4	J0940+0324	J094057.2+032401	0.060	43.12	1119 ± 95	810 ± 34	2249 ± 36	0.92 ± 0.09	5.98	−0.08
5	J1000+5536	J100032.2+553631	0.215	43.79	1065 ± 75	1216 ± 35	1056 ± 17	0.28 ± 0.10	6.76	−0.20
6	J1114+5258	J111443.7+525834	0.079	43.25	970 ± 60	866 ± 21	1158 ± 14	0.65 ± 0.08	6.04	−0.02
7	J1140+0307	J114008.7+030711	0.081	43.12	675 ± 41	571 ± 18	1337 ± 17	0.97 ± 0.08	5.69	0.200
8	J1231+1051	J123126.5+105111	0.304	43.92	957 ± 23	1200 ± 332	1143 ± 255	0.57 ± 0.05	6.93	−0.23
9	J1246+0222	J124635.2+022209	0.048	43.49	811 ± 27	709 ± 15	11669 ± 118	0.83 ± 0.04	6.09	0.171
10	J1331−0152	J133141.0−015213	0.145	43.56	1192 ± 42	1044 ± 16	1929 ± 15	0.35 ± 0.03	6.54	−0.20
11	J1357+6525	J135724.5+652506	0.106	43.14	737 ± 41	694 ± 16	1471 ± 16	0.45 ± 0.07	6.00	−0.08
12	J1415−0030	J141519.5−003022	0.134	43.36	1045 ± 27	954 ± 11	1735 ± 13	0.76 ± 0.04	6.40	−0.26
13	J2219+1207	J221918.5+120753	0.081	43.66	982 ± 38	886 ± 15	4369 ± 38	1.11 ± 0.06	6.32	0.115

Notes. Column 2: abbreviated name of objects; Column 3: SDSS name; Column 4: redshift; Column 5: monochromatic luminosity at 5100 Å (erg s^{-1}); Column 6: Hβ linewidth (km s^{-1}); Column 7: Hα linewidth (km s^{-1}); Column 8: Hα broad component flux (10^{-17} erg s^{-1} cm^{-2}); Column 9: the optical Fe II strength relative to the Hβ broad component; Column 10: black hole mass ($M_{\odot}$); Column 11: Eddington ratio.

properties of VNLS1s can be compared to AGNs with genuine small mass black holes, say, $M_{\mathrm{BH}} < 10^6\ M_{\odot}$ (e.g., Greene & Ho 2007a; Dewangan et al. 2008; Miniutti et al. 2009). This may provide possible insight into the black hole masses of VNLS1s and help distinguish different models of NLS1s (Osterbrock & Pogge 1985; Mineshige et al. 2000; Sulentic et al. 2000).

Although some VNLS1s have been studied in X-rays individually in the literature, systematic studies of their ensemble X-ray properties are rare, however, given the lack of homogeneously selected samples in the past. Recently, the X-ray properties of small samples of AGNs with $M_{\mathrm{BH}} \lesssim 10^6\ M_{\odot}$ with *XMM-Newton* observations have been presented (e.g., Dewangan et al. 2008; Miniutti et al. 2009), among which several objects are in fact VNLS1s considering their optical spectral properties and the high L/L_{Edd}. It was found that these VNLS1s are characterized by strong and rapid X-ray variability and soft X-ray excess emission. However, more observations for a larger, homogeneously selected sample are needed to confirm these results.

Using a large NLS1 sample selected from the Sloan Digital Sky Survey (SDSS), Zhou et al. (2006) found that, to their surprise, the previously known FWHM(Hβ)–Γ_{s} (soft X-ray photon index) anti-correlation becomes flat at FWHM $\sim$ 1200 km s^{-1}. Though in the small FWHM regime AGNs having flat Γ_{s} have previously been noted to exist,[5] the lack of expected steep soft X-ray slopes is intriguing. However, enhanced X-ray absorption in VNLS1s may explain such a trend, which, though it seems to be unlikely, cannot be ruled, since in Zhou et al. (2006) Γ_{s} (estimated from the *ROSAT* hardness ratios) are subject to large uncertainties. Detailed spectral modeling of the X-ray spectra with higher spectral resolutions and signal-to-noise ratios (S/N) for these objects is needed to confirm this interesting trend.

Motivated by the above considerations, here we present a study on the X-ray properties of a sample of NLS1 with extreme linewidth, FWHM $\leqslant$ 1200 km s^{-1}, using data from archival *XMM-Newton* observations. The sample and data reduction are described in Section 2. The modeling of the *XMM-Newton* spectra is presented in Section 3, with a focus on the soft X-ray excess. The X-ray temporal properties are presented in Section 4, followed by the effective optical to X-ray spectral indices. The results and their implications are discussed in Section 6 and are summarized in Section 7. We assume a cosmology with $H_0 = 70$ km s^{-1} Mpc^{-1}, $\Omega_{\Lambda} = 0.73$, and $\Omega_M = 0.27$. All quoted errors correspond to the 90% confidence level unless specified otherwise.

2. SAMPLE AND X-RAY DATA

2.1. X-ray VNLS1 Sample

We select VNLS1s from a large, homogeneous sample of ~2000 NLS1s built by Zhou et al. (2006; hereafter the Zhou'06 sample) from the SDSS DR3, which can be considered as basically optically selected. We adopt an operational linewidth cutoff of FWHM(Hβ) $\lesssim$1200 km s^{-1} for VNLS1s, in consideration of the fact that below roughly this value the Γ_{s}–FWHM anti-correlation becomes flat (see Figure 17 in Zhou et al. 2006). There are 384 NLS1s meeting this criterion. We match these VNLS1s with the 2XMM source catalog (Watson 2007) using a matching radius of 5″ and then select those detected in X-rays with at least 200 net source counts. We consider radio-quiet[6] objects only, since X-rays from radio-loud NLS1s may be contaminated by emission from relativistic jets (Zhou et al. 2007; Yuan et al. 2008; Abdo et al. 2009). The above selection results in 13 objects with reasonable S/N, which form our working sample of VNLS1s in this study. The sample objects are listed in Table 1, and the logs of the *XMM-Newton* observations are summarized in Table 2. Among the sample, the *XMM-Newton* data of seven objects are presented here for the first time, while the *XMM-Newton* spectra of six objects[7] have been presented previously in various detail in the literature for different aims. For the purpose of sample study using homogeneously derived results, we also re-analyze the *XMM-Newton* spectra of these objects, in the same way as for the other objects whose *XMM-Newton* data are presented for the first time here.

The optical spectral and continuum parameters of the sample objects are taken from Zhou et al. (2006) and given in Table 1.

[5] For such AGNs, their deviation from the above relation is explained as due to their low luminosity (low L/L_{Edd}); see Laor (2000).

[6] Having radio loudness less than 10, defined as the rest-frame flux ratio between the radio 1.4 GHz and the optical g band (see Zhou et al. 2006).

[7] They are J0107+1408, J1140+0307, J1357+6525 (Dewangan et al. 2008; Miniutti et al. 2009), J1246+022 (Porquet et al. 2004), J2219+1207 (Gallo et al. 2006), and J1415−0030 (Foschini et al. 2004).

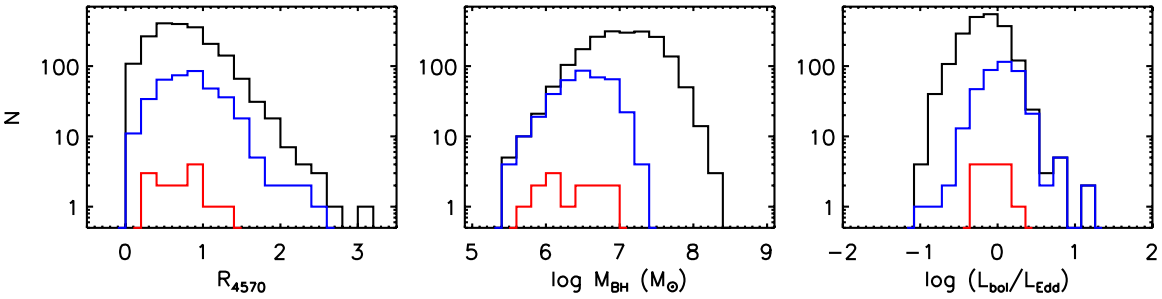

Figure 1. Distributions of the Fe II to Hβ flux ratio (R_{4570}), black hole mass and the Eddington ratio for our sample (red), the total Zhou'06 NLS1s sample (black), and the whole subsample with FWHM(Hβ) $\leqslant$1200 km s^{-1}(blue).

(A color version of this figure is available in the online journal.)

Table 2
Log of *XMM-Newton* Observations

Name	Date	Off-axis	Exposure Time			Note
			PN	MOS1	MOS2	
(1)	(2)	(3)	(4)	(5)	(6)	(7)
J0107+1408	2005 Jul 22	0.0	15.1	27.1	27.1	c
J0740+3118	2001 Apr 19	12.7	...	2.2	...	a
J0922+5120	2005 Oct 8	0.0	5.2	19.2	...	c
J0940+0324	2005 Oct 30	11.8	21.9	26.1	26.2	b
J1000+5536	2001 Apr 13	12.8	...	...	8.2	a
	2003 Oct 14	13.5	14.2	...	...	a
J1114+5258	2003 Apr 25	11.3	3.9	6.6	7.0	a
J1140+0307	2005 Dec 3	0.0	30.8	38.5	39.2	c
J1231+1051	2003 Jul 13	12.0	...	45.3	...	a
	2005 Dec 13	12.0	...	...	68.2	a
	2005 Dec 17	12.0	...	91.6	91.6	a
J1246+0222	2001 Jun 17	0.0	3.1	...	...	c
J1331−0152	2001 Jul 29	12.0	...	32.3	32.3	b
J1357+6525	2005 Apr 4	0.0	14.5	21.1	20.6	c
J1415−0030	2003 Feb 8	10.0	9.5	13.7	14.2	b
J2219+1207	2001 Jun 7	0.1	7.2	...	...	c

Notes. Column 2: observation date; Column 3: off-axis angle in arcmin; Columns 4–6: cleaned exposure time of the three EPIC cameras in kilosecond; Column 7: energy range in which the source spectrum is extracted—(a) 0.2–2.4 keV, (b) 0.2–7 keV, and (c) 0.2–10 keV.

The black hole masses are estimated from the broad component of the Hα line using the $M_{\rm BH}$–linewidth–luminosity relation in Greene & Ho (2007b). We also estimate the Eddington ratio $L/L_{\rm Edd}$ assuming the bolometric luminosity as $9\lambda L_{5100}$ (Elvis et al. 1994), where λL_{5100} is the monochromatic luminosity at 5100 Å. Figure 1 shows the distributions of several parameters of our working sample, namely, $M_{\rm BH}$, $L/L_{\rm Edd}$, and the optical Fe II emission multiplets strength R_{4570},[8] in comparison with those of the NLS1 sample of Zhou'06 as well as the overall FWHM $<$1200 km s^{-1} (VNLS1) subsample. A few remarks can be made concerning the bulk properties of the sample. First, both of these two VNLS1 subsamples have similar R_{4570} distributions to that of the parent sample, confirming their typical NLS1 nature. The general strong Fe II emission is also demonstrated in the composite SDSS spectrum of our *XMM-Newton* VNLS1 sample (Figure 2). Second, our VNLS1s have lower $M_{\rm BH}$ and higher $L/L_{\rm Edd}$ distributions in general than the overall NLS1 sample, as expected from their narrower linewidths. Third, our

[8] Defined as the Fe II($\lambda\lambda$4434 − 4684) to Hβ flux ratio, where Fe II($\lambda\lambda$4434 − 4684) denotes the flux of the Fe II multiplets integrated over the wavelength range of 4434–4684 Å, and Hβ the flux of the broad component of Hβ; see Zhou et al. (2006).

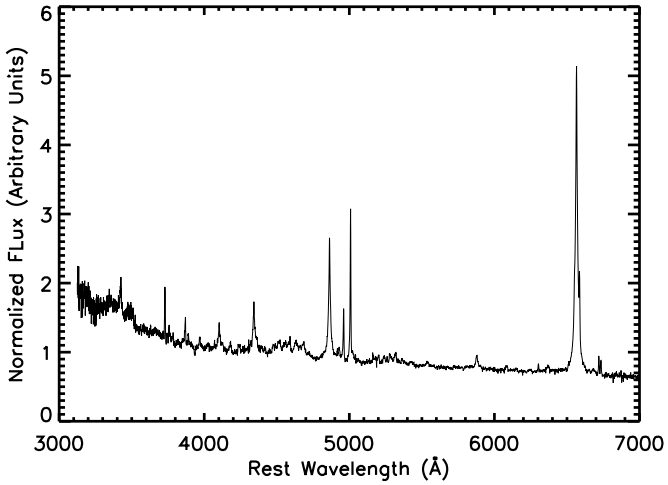

Figure 2. Composite optical spectrum of our sample objects derived from their individual SDSS spectra. The strong Fe II multiplet emission is characteristic of typical NLS1 spectra.

XMM-Newton sample is roughly consistent with the overall VNLS1s in these distributions. Thus, our X-ray VNLS1 sample is not biased from, but rather representative of, optically selected NLS1s with the smallest linewidth. This should be kept in mind when comparing our results with those obtained in previous studies, especially for X-ray-selected NLS1 samples.

2.2. X-ray Observations and Data Reduction

The observational data with *XMM-Newton* were retrieved from the *XMM-Newton* Science Archival Center. For all but one object the observations were operated in the full window mode. For the only exception, J2219+1207, the MOS cameras were operated in the small window mode, in which a considerable fraction of the source counts in the wing of the point-spread function (PSF) were lost, and thus only the PN data are used. The PN observation of J1246+0222 experienced a pile-up, which is corrected by excising the core of the PSF with a radius of 10″. Some of the data of the individual cameras as listed in Table 2 cannot be utilized due to the sources being either at the edges or in the gaps of the CCDs, out of the field of view, or on a bad CCD column.

For *XMM-Newton* data reduction we use the standard Science Analysis System (SAS; v8.1.0.). The Observation Data Files are processed to create calibrated events files with "bad" (e.g., "hot," "dead," "flickering") pixels removed. The time intervals of high flaring background contamination are identified and subsequently removed following the standard SAS procedures and thresholds. Source counts are extracted from a circle with

Table 3
XMM-Newton Spectral Fits with an Absorbed Power-law Model

Name (1)	$N_{\rm H}^{\rm Gal}$ (2)	$N_{\rm H}^{\rm in}$ (3)	$\Gamma_{\rm soft}$ (4)	log $L_{\rm soft}$ (5)	χ^2_ν/dof (6)	$\Gamma_{\rm hard}$ (7)	log $L_{\rm hard}$ (8)	χ^2_ν/dof (9)	EW (10)
J0107+1408	3.37	4.2 ± 0.8	2.63 ± 0.08	43.07	1.0/230	2.26 ± 0.22	42.47	1.3/44	<45
J0740+3118	4.32	...	3.38 ± 0.30	44.72	c-stat	...	...	...	...
J0922+5120	1.20	2.7 ± 0.5	3.72 ± 0.07	44.23	1.7/226	2.28 ± 0.36	43.31	1.3/24	<228
J0940+0324	3.25	...	2.43 ± 0.03	43.00	1.0/244	$2.02^{+0.19}_{-0.25}$	42.56	1.1/39	<497
J1000+5536	0.83	...	2.03 ± 0.38	43.33	c-stat	...	...	...	...
	...	...	2.34 ± 0.25	43.14	1.5/18	...	...	...	...
J1114+5258	0.99	...	2.77 ± 0.07	43.16	0.8/60	...	...	...	...
J1140+0307	1.88	1.3 ± 0.2	2.89 ± 0.03	43.44	1.3/375	2.06 ± 0.13	42.65	1.0/94	<111
J1231+1051	2.40	...	2.89 ± 0.18	44.10	0.9/26	...	...	...	...
	...	...	2.80 ± 0.16	43.83	1.5/28	...	...	...	...
	...	...	2.90 ± 0.07	43.93	1.0/69	...	...	...	...
J1246+0222	1.74	1.83 ± 0.5	2.97 ± 0.06	43.65	1.2/198	$2.25^{+0.35}_{-0.23}$	42.74	1.1/17	<214
J1331−0152	2.33	...	2.67 ± 0.05	43.65	1.0/58	$1.95^{+0.69}_{-0.35}$	43.18	0.8/11	<361
J1357+6525	1.21	2.3 ± 0.4	2.68 ± 0.06	43.43	1.1/265	$2.29^{+0.16}_{-0.32}$	42.85	1.1/46	<276
J1415−0030	2.84	...	2.76 ± 0.06	43.49	1.0/104	$2.21^{+0.51}_{-0.47}$	42.81	1.4/11	<842
J2219+1207	4.81	2.8 ± 0.7	3.15 ± 0.07	44.19	1.0/264	2.39 ± 0.16	43.21	1.1/38	<125

Notes. Column 2: Galactic column density in 10^{20} cm^{-2}; Column 3: column density of intrinsic neutral absorption in the object's rest frame in 10^{20} cm^{-2}; Column 4: fitted power-law photon index in the soft X-ray band (0.2–2.4 keV); Column 5: absorption corrected luminosity in 0.2–2.4 keV in erg s^{-1}; Column 6: reduced χ^2; Column 7: fitted power-law photon index in the hard X-ray band (mostly in 2–10 keV; see Table 2); Column 8: absorption corrected luminosity in 2–10 keV in erg s^{-1}; Column 9: reduced χ^2; Column 10: rest-frame equivalent width of the Fe Kα line in units of eV.

a radius ranging from, depending on the source position on the detector, 30″ to 65″ at the source position, and the background counts from a source-free region with a usually larger radius. To extract X-ray spectra only X-ray events with the pattern $\leqslant$4 for PN and $\leqslant$12 for MOS are used. Background-subtracted light curves are also extracted from cleaned event files and are subsequently corrected for instrumental effects (such as vignetting and dead time) using the SAS task "epiclccorr."

When both are available, the two MOS spectra of each observation are all found to be well consistent with each other, and are therefore co-added to form a single MOS spectrum to increase the S/N (using the FTOOLS addspec 1.3.0). We set the low-energy cutoff of the spectra to 0.2 keV, following the recommendation of the most recent EPIC calibration status report (Guainazzi 2010). The high-energy cutoff is set such that above roughly this energy the background spectrum starts to dominate. Since there is a diverse range of the spectral S/N, the high-energy cutoff varies among the sample objects. For four objects with low spectral S/N, only the 0.2–2.4 keV range is used. For the remaining nine objects, the high-energy cutoff of either 7 keV or 10 keV is used, depending on the spectral quality (see Table 2). The EPIC spectra are then grouped in a way that there are at least 25 counts in each energy bin. Spectral fitting is performed using XSPEC (v.12.3; Arnaud 1996). Whenever both PN and MOS spectra are available for an observation, we perform joint spectral fitting with all the same spectral parameters tied together except the normalization.

3. X-RAY SPECTRA ANALYSIS

3.1. Continuum Shape and Fe Kα Emission Line

In order to compare the X-ray continuum slopes with results from other previous AGN studies, we first characterize the X-ray spectral shape with an absorbed power-law model in both the soft (0.2–2.4 keV) and "hard" (2–10 keV) bands.[9] The results are listed in Table 3. In the soft X-ray band, the model with a neutral absorption column density ($N_{\rm H}$) fixed at the Galactic value ($N_{\rm H}^{\rm Gal}$) yields acceptable fit for about half of the sample objects. In the remaining objects, the fit can be improved by adding an extra neutral absorber in the objects' rest frame. The fitted excess absorption $N_{\rm H}$ is small, however, comparable to $N_{\rm H}^{\rm Gal}$. In only one object, J1415−0030, ionized absorption is required to yield acceptable fit, with an edge-like feature around 0.6 keV (see Section 3.2). We conclude that intrinsic absorption is not significant in these objects. We thus suggest that the observed flattening of the FWHM(Hβ)–$\Gamma_{\rm s}$ relation below FWHM $\sim$1200 km s^{-1} as found in Zhou et al. (2006) is not caused by X-ray absorption, but is most likely an intrinsic property. For those having more than one measurement, there seems to be little or no changes in the soft X-ray spectral shape, and the mean $\Gamma_{\rm s}$ are calculated. The fitted $\Gamma_{\rm s}$ values range from 2.03 to 3.72. We quantify the intrinsic distribution of $\Gamma_{\rm s}$ (assumed to be Gaussian) that is disentangled from measurement errors using the maximum-likelihood method as first applied by Maccacaro et al. (1988); we find a mean $\langle\Gamma_{\rm s}\rangle = 2.83^{+0.19}_{-0.20}$, and a standard deviation $\sigma = 0.31^{+0.20}_{-0.10}$ (90% confidence), whose confidence contours are shown in Figure 3.

In the hard X-ray band there are nine objects having high enough spectral S/N for measuring photon indices $\Gamma_{\rm h}$. The absorption $N_{\rm H}$ is fixed at the Galactic value. A power law can well reproduce the observed hard X-ray spectrum in five objects, whereas the remaining four objects (J0922+5120, J1140+0307, J1246+0222, and J2219+1207) show a possible broad excess emission feature in the residuals around 5 keV. The fitted $\Gamma_{\rm h}$ values are in the range of 1.95–2.39. The maximum-likelihood intrinsic distribution of $\Gamma_{\rm h}$ has a mean of $\langle\Gamma_{\rm h}\rangle = 2.19^{+0.19}_{-0.18}$, which is flat for typical NLS1s, and a small intrinsic scatter, $\sigma = 0.0^{+0.29}_{-0.0}$ (see Figure 3 for their confidence contours).

No Fe Kα emission line feature appears to be present in all the objects except J1357+6525, which shows a marginal feature of a narrow line at around 6.4 keV. For this object adding a Gaussian (to an absorbed power-law model in the 2–10 keV band) slightly improved the fit, though with only $\Delta\chi^2 = 5$ for

[9] For three objects only the 2–7 keV band is used since the spectra above 7 keV are dominated by backgrounds; see Table 2.

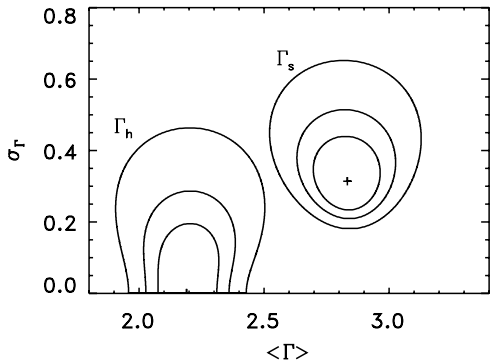

Figure 3. Confidence contours (at the 68%, 90%, and 99% confidence levels) of the mean and standard deviation of the intrinsic distributions (assumed to be Gaussian) of the soft (Γ_s) and hard (Γ_h) X-ray photon indices for our VNLS1, which are derived using the maximum-likelihood method (see the text). Pluses indicate the best-estimated values.

3 degrees of freedom (dof), i.e., the addition of an extra Gaussian component is not statistically significant. Thus only upper limits can be derived on the EW of any potentially narrow Fe Kα line at 6.4 keV (assuming $\sigma = 10$ eV). The derived upper limits at the 90% significance are given in Table 3. We compared our objects with the Fe Kα line EW and X-ray luminosity relation for AGNs as given in Page et al. (2004) and found that the derived line EW limits are well consistent with the relation.

3.2. Soft X-ray Excess

A comparison of the soft and hard X-ray spectral indices obtained above indicates an overall spectral steepening toward low energies in *all* of the objects, suggesting the presence of the soft X-ray excess. As a demonstration, we show in Figure 4 the X-ray spectra of the four VNLS1s, which are presented for the first time, and the extrapolation down to 0.2 keV of the power-law model fitted in the hard X-ray band. Significant excess emission in the soft X-ray band is prominent, similar to that reported in the other objects of the sample (e.g., Miniutti et al. 2009), which is also confirmed here. We thus conclude that the apparent soft X-ray excess emission is ubiquitous in our VNLS1 sample.

Given the small $M_{\rm BH}$ and high accretion rate ($L/L_{\rm Edd}$) in VNLS1s, the expected blackbody emission from accretion disks is shifted toward higher energies compared to classical AGNs with more massive black holes, and the high-energy turnover may start to emerge in the soft X-rays (e.g., $kT_{\rm max} \sim 72$ eV for J0940+0324 assuming a Schwarzschild black hole; e.g., Peterson 1997). Thus the blackbody emission directly from the disks might be detected. We first model the soft X-ray excess with a blackbody. The model yields acceptable or marginally acceptable fits for all except for two objects. For J0107+1408 an additional neutral absorber is required to improve the fit. For J1415−0030 a moderately ionized absorber is needed; adding an absorption edge improves the fit significantly with $\Delta\chi^2 = 12$ for

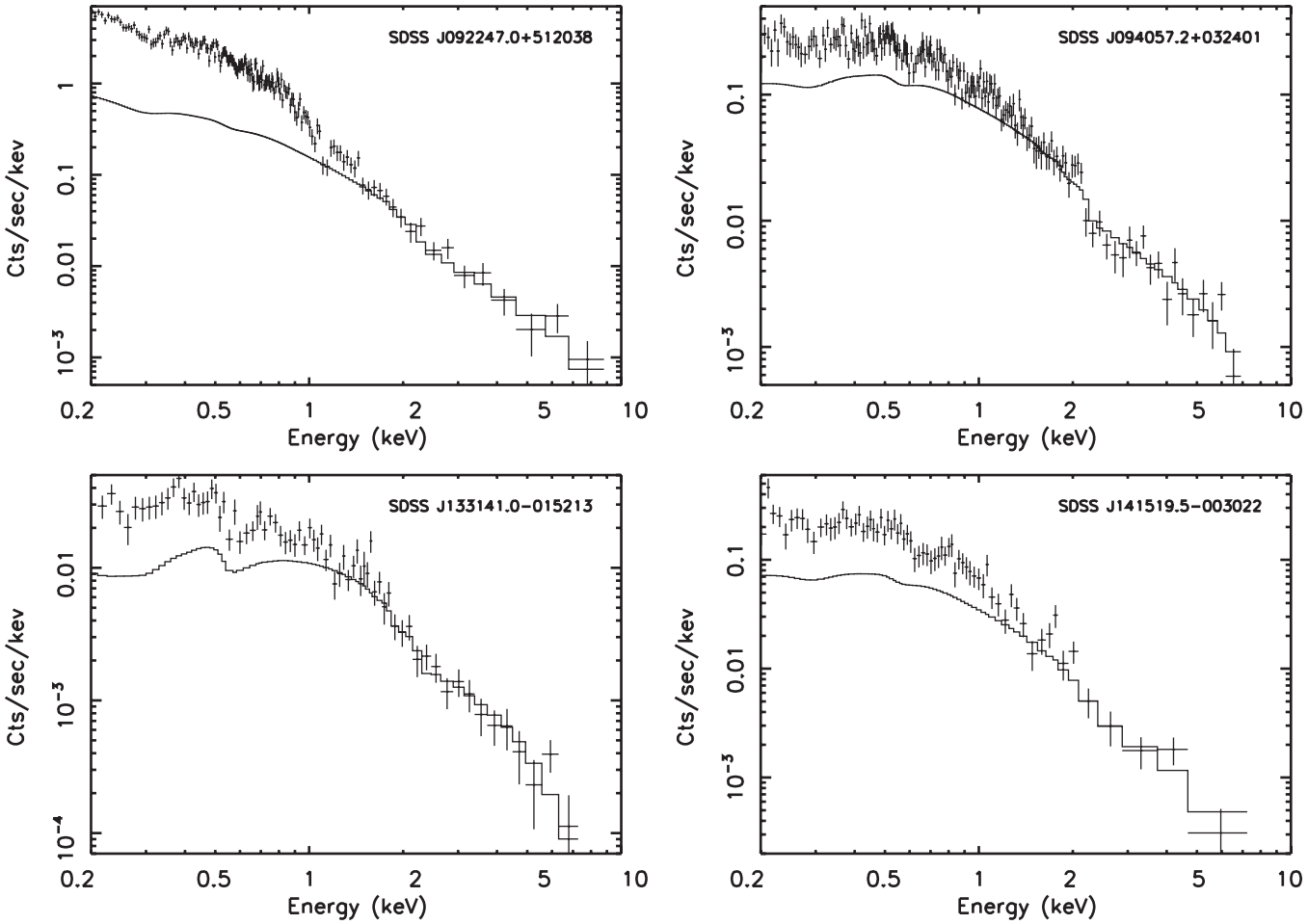

Figure 4. *XMM-Newton* spectra of the four objects among our VNLS1 sample (PN spectra except for J1331−0152 of which MOS spectra are used). The power-law model fitted to 2–10 keV spectra and its extrapolation to the soft X-ray band is also shown. Soft X-ray excess emission is clearly present.

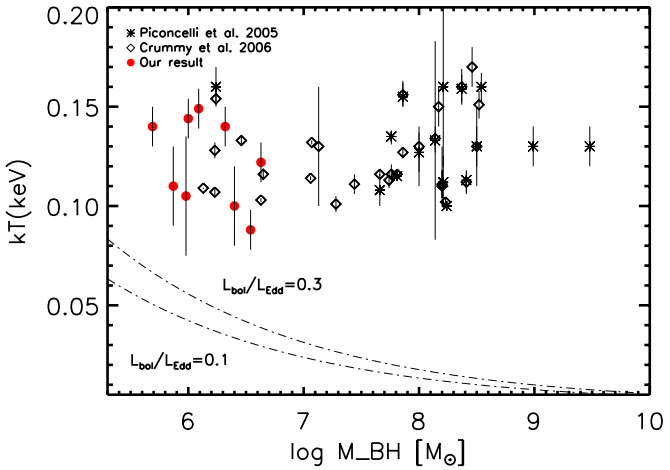

Figure 5. Observed temperature of the soft excess is plotted vs. the black hole mass. Filled circles are our results, stars for the radio-quiet PG quasars (Piconcelli et al. 2005), and diamonds for type 1 AGNs (Crummy et al. 2006). The dotted-dashed lines are the maximum temperature expected from the accretion disk.

(A color version of this figure is available in the online journal.)

three additional free parameters. The fitted edge energy is 0.67 ± 0.03 keV with an optical depth of 0.55 ± 0.2, corresponding to the K-shell binding energy of ionized oxygen ions.

The fitted temperatures are in the range of 100–200 eV (Table 4), in agreement with those found in AGNs having more massive black holes of 10^7–10^9 $M_\odot$ (Gierliński & Done 2004; Porquet et al. 2004; Crummy et al. 2006; Bianchi et al. 2009). Hence, our results confirm the extension of the canonical 100–200 eV temperatures down to AGNs with $M_{\rm BH}$ as low as around $\sim 10^6$ $M_\odot$ (Miniutti et al. 2009) by adding more objects in this $M_{\rm BH}$ range. The result is clearly demonstrated in Figure 5, in which our results are compared with those of AGNs and quasars with more massive black holes (Piconcelli et al. 2005; Crummy et al. 2006). These values are still systematically higher than the maximum temperatures predicted for standard accretion disks. The independence of the thermal temperature on $M_{\rm BH}$ over such a wide $M_{\rm BH}$ range argues against the direct blackbody emission from accretion disks as the origin of the observed soft X-ray excess for the vast majority of AGNs, except for RX J1633+4718 (Yuan et al. 2010).

Recent studies suggest that, similar to the blackbody temperature, the relative strength of the soft X-ray excess also falls within a relatively small range for Palomar-Green (PG) quasars (Piconcelli et al. 2005) and Seyfert 1 AGNs (Middleton et al. 2007) and AGNs with small masses (Miniutti et al. 2009). Here we examine this quantity for the VNLS1s of our sample. We estimate the relative strength as the luminosity ratio of the excess component, modeled as a blackbody, to the total luminosity in the 0.5–2 keV band. The values are in the range of 8%–38% with a mean of 21% (Table 4). Apparently, when combined with previous results, as shown in Figure 6, there seems no strong dependence on the Hβ linewidth over a large range, FWHM(Hβ) = 600–10,000 km s^{-1} (a Spearman correlation test probability of 0.79). The mean relative strength of our VNLS1s is somewhat smaller than that of the PG quasars (31%) in Piconcelli et al. (2005) derived from their fitting results, though further confirmation is needed given the relatively small size of our sample.

There are currently several viable models to account for the soft X-ray excess. Photon trapping in high accreting system where advection is important (Abramowicz et al. 1988), or Comptonization of ultraviolet photon from the accretion disk by

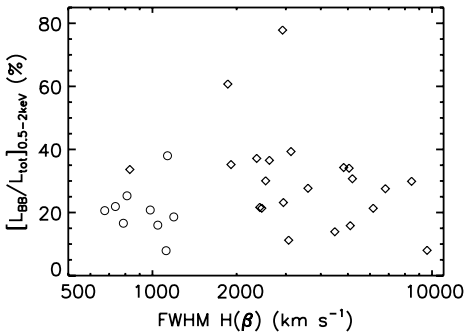

Figure 6. Soft X-ray excess strength, parameterized as the ratio of the blackbody to the total luminosity in the 0.5–2 keV range, vs. the linewidth for the VNLS1s in our sample (open circles) and the radio-quiet PG quasars (diamonds) in Piconcelli et al. (2005).

electrons as hotter skin above the disk (Czerny & Elvis 1987; Wandel & Petrosian 1988; Shimura & Takahara 1993; Czerny et al. 2003), can explain the required higher temperature. On the other hand, absorption or emission lines arising from atomic processes, when blurred due to relativistic motion, can mimic the soft X-ray excess. For example, strong relativistically blurred emission/absorption lines between $\sim$0.7–2 keV due to O VII/O VIII and Fe transitions can be produced from ionized disk illuminated by an underlying hard X-ray continuum (reflection) in the vicinity of the central black hole (Ross & Fabian 1993), or from disk winds (Gierliński & Done 2004). Below we investigate these models by fitting them to the soft X-ray excess spectra. In the spectral fitting, a power-law continuum modified by neutral absorption with $N_{\rm H}$ fixed at the Galactic value is always included. For objects whose data have been analyzed previously, we compare our results with previous results individually in the appendix.

3.2.1. Comptonization

We use the Comptonization model (*comptt* in XSPEC; Titarchuk 1994) and fix the input seed photon energy at the innermost temperature of the standard accretion disk based on the estimation of the black hole masses and accretion rates ($L/L_{\rm Edd}$). In this case, the emergent spectral shape depends on only two parameters, the temperature and the optical depth of scattering electrons. This model gives significantly improved fits over, or at least as good as, the above blackbody fits for all of the objects (see Table 4, Figure 7). The inferred electron temperatures are found in a relatively small range, $kT_{\rm plasma} \sim$ 0.17–0.30 keV, and the optical depth $\tau \sim$ 10–25.

3.2.2. Disk Reflection

We use the latest ionized disk reflection model from Ross & Fabian (2005; *reflion* in XSPEC) and in the fits the photon indices of the ionizing continuum and the observed continuum are tied together, and solar abundance is assumed. For relativistic blurring the Laor kernel model (*kdblur* in XSPEC; Laor 1991) is used with an outer radius fixed at 400 r_g, an emissivity index of the disk fixed to the standard value of 3, and the inner disk radius allowed to vary. Although this model can reproduce acceptable fitting results for most of the objects, in three objects the residuals in the soft X-rays indicate possible contribution from another component. Following Miniutti et al. (2009), we then include an additional blackbody component in the fits to account for possible contribution from the accretion disk. This improves the fits for all of the three, namely, J0107+1408 ($\Delta\chi^2$/dof = 14/3), J0922+5120 ($\Delta\chi^2$/dof = 204/3), and J2219+1207 ($\Delta\chi^2$/dof =

Table 4
Results of Spectral Fits in 0.2–10 keV with Different Models for the Soft Excess

Blackbody						
Name	Γ	kT (keV)	BB/Total[a]	χ^2/dof		
J0107+1408	$2.39^{+0.08}_{-0.10}$	0.11 ± 0.02	0.166	277/264		
J0922+5120	3.18 ± 0.09	0.12 ± 0.01	0.380	356/255		
J0940+0324	2.29 ± 0.05	$0.11^{+0.04}_{-0.03}$	0.079	278/273		
J1140+0307	2.56 ± 0.04	0.14 ± 0.01	0.206	570/472		
J1246+0222	2.61 ± 0.02	0.15 ± 0.01	0.253	220/212		
J1331−0152	2.27 ± 0.06	0.09 ± 0.01	0.186	61/68		
J1357+6525	2.36 ± 0.09	0.14 ± 0.01	0.219	319/303		
J1415−0030	$2.42^{+0.12}_{-0.20}$	0.10 ± 0.02	0.160	102/109		
J2219+1207	2.70 ± 0.04	0.14 ± 0.01	0.208	293/293		
Comptonization						
Name	Γ	$kT_{\rm plasma}$ (keV)	τ	χ^2/dof		
J0107+1408	2.32 ± 0.06	0.25 ± 0.07	10.9 ± 4.3	272/263		
J0922+5120	2.09 ± 0.19	0.17 ± 0.01	$19.9^{+2.5}_{-0.6}$	325/254		
J0940+0324	2.04 ± 0.19	0.30 ± 0.10	13.5 ± 2.1	269/272		
J1140+0307	2.19 ± 0.15	0.22 ± 0.03	18.7 ± 7.9	540/471		
J1246+0222	2.34 ± 0.23	0.21 ± 0.02	21.0 ± 5.5	217/211		
J1331−0152	2.12 ± 0.21	0.17 ± 0.07	17.1 ± 7.9	60/67		
J1357+6525	2.22 ± 0.04	0.19 ± 0.02	23.5 ± 7.0	320/302		
J1415−0030	2.04 ± 0.20	0.20 ± 0.06	20.0 ± 4.8	99/108		
J2219+1207	2.36 ± 0.15	0.21 ± 0.04	18.1 ± 7.0	279/292		
Disk Reflection						
Name	Γ	$r_{\rm in}/r_g$	logξ	kT (keV)[b]	Flux Frac[c]	χ^2/dof
J0107+1408	2.24 ± 0.17	$4.93^{+3.31}_{-}$	3.45 ± 0.4	0.05 ± 0.008	0.3	260/259
J0922+5120	2.41 ± 0.25	$1.73^{+11.07}_{-}$	$3.33^{+0.13}_{-0.12}$	0.06 ± 0.01	0.5	257/250
J0940+0324	2.16 ± 0.12	$1.41^{+8.98}_{-}$	$3.76^{+}_{-0.21}$	...	0.9	273/271
J1140+0307	2.38 ± 0.08	$3.86^{+0.89}_{-}$	$3.83^{+0.05}_{-0.15}$	...	0.9	524/470
J1246+0222	2.43 ± 0.10	$3.82^{+2.32}_{-}$	$3.75^{+}_{-0.19}$	...	1.0	212/210
J1331−0152	2.29 ± 0.25	$1.24^{+3.15}_{-}$	$3.27^{+}_{-0.25}$	...	0.3	69/66
J1357+6525	2.19 ± 0.07	$6.05^{+1.91}_{-3.03}$	$3.28^{+0.30}_{-0.23}$	...	0.5	320/301
J1415−0030	2.24 ± 0.24	$1.25^{+2.24}_{-}$	$3.13^{+0.12}_{-0.43}$	...	0.7	104/109
J2219+1207	2.43 ± 0.05	$4.46^{+2.15}_{-}$	$3.79^{+}_{-0.15}$	$0.08^{+0.01}_{-0.03}$	0.8	272/289
Smeared Absorption						
Name	Γ	log ξ	$N_{\rm H}$ (10^{22} cm^{-2})	σ (v/c)	χ^2/dof	
J0107+1408	2.47 ± 0.21	3.00 ± 0.71	12^{+}_{-6}	$0.50^{+}_{-0.16}$	278/264	
J0922+5120	2.69 ± 0.07	3.11 ± 0.04	50^{+}_{-2}	$0.5^{+}_{-0.05}$	388/255	
J0940+0324	2.22 ± 0.10	3.46 ± 0.35	35^{+}_{-24}	$0.44^{+}_{-0.28}$	275/273	
J1140+0307	2.37 ± 0.03	3.40 ± 0.05	50^{+}_{-3}	$0.5^{+}_{-0.05}$	607/472	
J1246+0222	2.56 ± 0.09	3.58 ± 0.10	50^{+}_{-8}	$0.47^{+}_{-0.08}$	291/211	
J1331−0152	2.42 ± 0.07	2.75 ± 0.36	14^{+25}_{-9}	$0.5^{+}_{-0.19}$	60/67	
J1357+6525	2.26 ± 0.06	3.59 ± 0.06	50^{+}_{-9}	$0.5^{+}_{-0.24}$	359/303	
J1415−0030	2.60 ± 0.12	3.52 ± 0.50	9^{+}_{-5}	$0.49^{+}_{-0.16}$	112/110	
J2219+1207	2.60 ± 0.20	3.43 ± 0.03	50^{+}_{-5}	$0.5^{+}_{-0.05}$	320/292	

Notes. For SDSS J0107+1408 with free absorption in the fitting. For SDSS J1415−0030 an additional ionized absorption is applied (see the text). The blank parameter errors denote that the upper or lower limits are outside of the tabulated parameters range, which are considered to be not physically meaningful.

[a] Luminosity ratio of the blackbody component to the total component in 0.5–2 keV.

[b] Inferred temperatures of an additional blackbody component.

[c] Flux ratio of the reflected component to the total component in 0.2–10 keV.

24/2), with the addition of the blackbody component being statistically significant (a probability level <0.05 using the F-test). The inferred temperatures are 0.05 ± 0.008 keV, 0.06 ± 0.02 keV, and $0.08^{+0.01}_{-0.03}$ keV, respectively, broadly consistent with the maximum temperatures at near the inner disk predicted from the estimated black hole masses and accretion rates.

The disk reflection model, either with or without additional blackbody emission, provides acceptable fits for all and the best fits for some of the objects (see Figure 7 and Table 4). The best-fit disk inner radius is less than $6r_g$, suggesting a highly spinning Kerr black hole for most of our objects. The inferred disk inclination varies from 0° to 50°. The ionization parameters are log $\xi \sim 3.13$–3.83. We define a parameter "flux fraction" as the flux ratio of the reflected component to the total component over the range 0.2–10 keV (following Crummy et al. 2006). As can be seen in Table 4, in most of the objects where this model gives a good fit, the reflection component largely dominates the total observed flux in the 0.2–10 keV band.

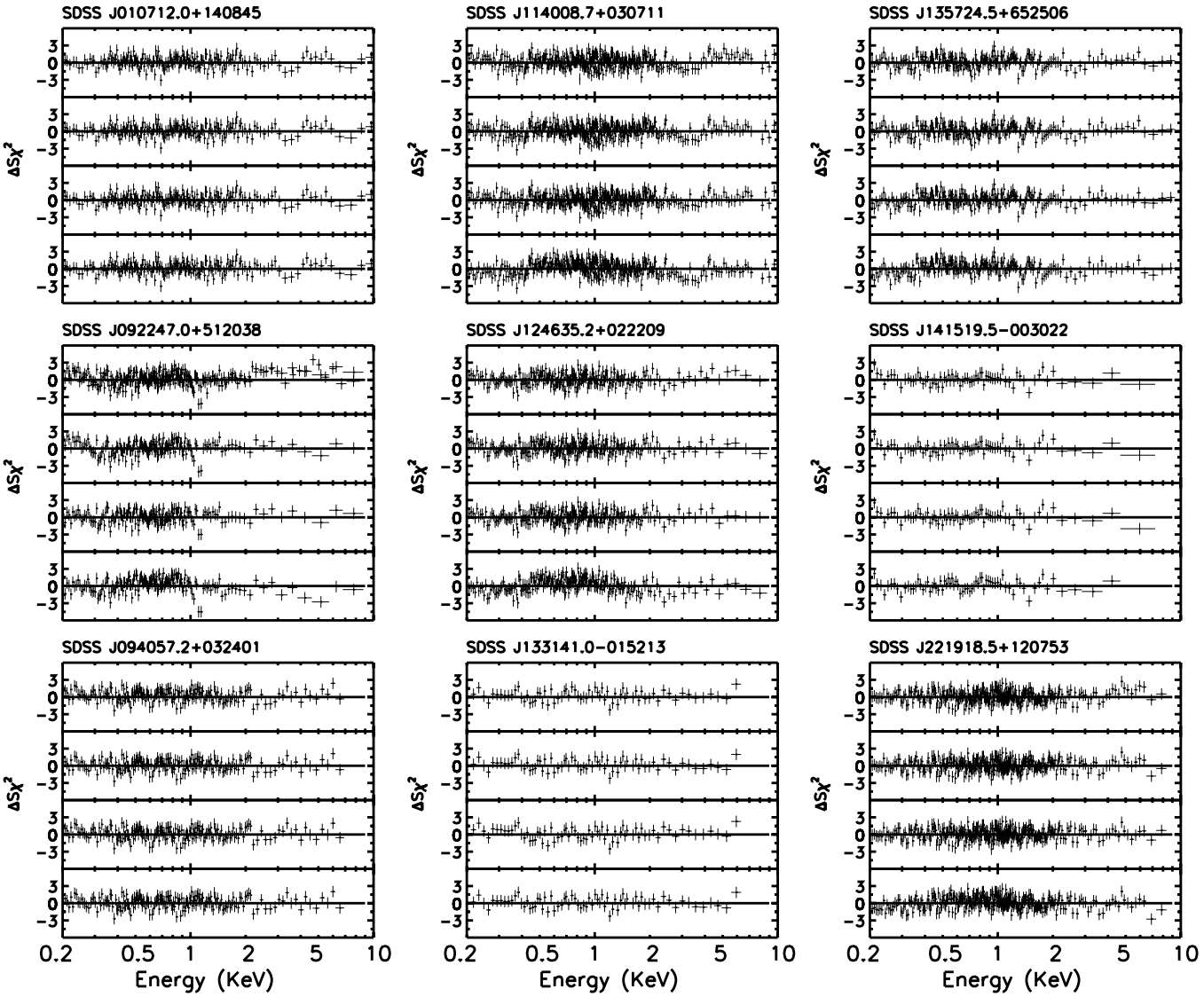

Figure 7. Residuals of spectral fits to the *XMM-Newton* spectra with various models to account for the soft X-ray excess, which are, from top to bottom for each panel, blackbody, Comptonization, disk reflection, and smeared absorption model. An additional blackbody component is added in the disk reflection model for J0107+1408, J0922+5120, and J2219+1207.

3.2.3. Smeared Absorption Model

Finally, we fit the spectra with the relativistically smeared absorption model (*swind1* in XSPEC). This model provides acceptable fits for nearly half of the objects but not for the remaining objects (Table 4, Figure 7). The inferred column densities are in the range of $N_{\rm H} \sim (0.9–5) \times 10^{23}$ cm^{-2}, the ionization parameters $\log \xi \sim 2.75–3.59$, and the smearing terminal velocities are very high, close to 0.5 c.

3.2.4. p-free Model

In this work, we also try the p-free disk model (*diskpbb* in XSPEC) to account for the soft excess. For some of the objects, this model gives fits as good as the Comptonization model, with the inferred temperatures at the inner disk radius of 0.15–0.35 keV, and the index of the temperature profile $p =$ 0.32–0.64. However, the innermost disk radii derived from the fitted normalization are significantly less than the estimated gravitational radii, even after the correction for the spectral hardening factor (∼1.9 as recommended by Kawaguchi 2003 for AGNs with Eddington ratios around 1). We thus consider the p-free model to be physically unrealistic and hence no fitted parameters are listed here.

3.2.5. Summary of Soft X-ray Excess Modeling

In general, the soft X-ray excess of these VNLS1s can be reproduced by more than one model, which often cannot be distinguished based on fitting statistics. However, disk reflection and/or Comptonization are much more preferred than the two other ones, i.e., the smeared absorption model with marginally improved fitting and the p-free model which is physically unrealistic. In the modeling of the X-ray spectra, no additional intrinsic absorption is required for all the objects except J0107+1408 and J1415-0030, of which additional neural and warm absorptions are needed, respectively.

For SDSS J0107+1408, neutral absorption with $N_{\rm H} \sim (6.55–11.41) \times 10^{20}$ cm^{-2} is required. For J1415−0030, in the above spectral fittings for this object with various soft X-ray excess models, we add ionized absorption (*zxipcf* in XSPEC) applicable to all the emission components. The overall spectrum and the edge feature can be well reproduced and all the

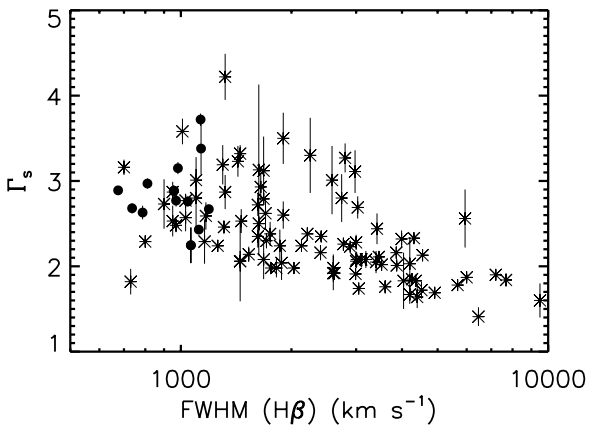

Figure 8. Soft X-ray photon index Γ_s vs. Hβ linewidth relation for our VNLS1s (filled circles). Stars are the results from Grupe et al. (2010).

fits are improved significantly, with a decrease of $\Delta\chi^2 = 10$ in general. The covering fraction of the absorber is close to unity, the absorbing column density is in the range of (9.3–15.8) $\times 10^{20}$ cm^{-2}, and the ionization parameter is $10^{0.21}$–$10^{0.38}$, depending on the exact model for the soft X-ray excess.

3.3. Γ_s–*FWHM Relation*

We have shown above that there is little or no significant intrinsic absorption in the X-ray spectra of most of these VNLS1s. Therefore the photon indices derived in Zhou et al. (2006) from the *ROSAT* hardness ratios are mostly reliable, and hence the spectral flattening toward the lower FWHM end (Zhou et al. 2006) is likely real, rather than being caused by X-ray absorption. Recently, Grupe et al. (2010) have studied the spectral indices of a sample of soft X-ray-selected AGNs measured with the *Swift* XRT, some of which also have linewidths similar to ours. We compare the soft X-ray photon indices of our VNLS1s with those of the Grupe et al. (2010) sample, as shown in Figure 8. It can be seen that in the lowest linewidth regime our Γ_s values are statistically compatible with the result of Grupe et al. (2010).[10] It also appears that there is a lack of AGNs having both narrow FWHM ($\lesssim$1000 km s^{-1}) and very steep soft X-ray spectra ($\Gamma_s \gtrsim 3.5$). This is consistent with the result suggested by Zhou et al. (2006). Using the combined data points in Figure 8, we test explicitly whether there exists a significant flattening in the Γ_s–FWHM relation at FWHM $\lesssim$ 1000 km s^{-1} using various methods; the result is inconclusive in the statistical sense, however. This might be partly due to the relatively small sample size and/or the heterogeneity of the combined samples. A larger and homogeneously selected sample is needed to test the possible deviation of this well-known Γ_s–FWHM relation at the low-FWHM end in the future.

4. X-RAY VARIABILITY

Figure 9 shows, as examples, the 0.2–10 keV light curves for the five objects in our sample, which are presented for the first time.[11] In fact, we find that, for most of the sample objects, the X-ray flux varied by more than a factor of 2 on timescales of 1–2 hr within the observational intervals. We conclude that short timescale variability is common to VNLS1s. Remarkable flux variations in short timescales are evident. We also investigate possible spectral variability within the observational intervals, which are divided into time bins, using the hardness ratios; however, no conclusive remarks can be made mainly due to the insufficient S/N of the data for such a purpose.

The X-ray variability amplitude can be characterized by the excess variance,[12] which has been found to be strongly correlated with the black hole masses (Lu & Yu 2001; Papadakis 2004; O'Neill et al. 2005). Using the *XMM-Newton* data, some are included in the current sample; Miniutti et al. (2009) extended this relation to AGNs with black hole masses $< 10^6\ M_\odot$ (three included in our sample) and demonstrated that the relationship is relatively tight. This result indicates that black hole mass is a primary parameter that drives the relative X-ray variability in AGNs. In the same way as in Miniutti et al. (2009), we calculate the excess variance for the four objects not presented previously that makes use of light curve segments of equal duration (20 ks) and equal time bin size (500 s) in the 2–10 keV band. However, for only one object, J0922+5120, the light curve has S/N high enough to yield reliably determined excess variance, $\log\sigma^2_{\rm NXS} = -1.15 \pm 0.68$. We locate this object ($M_{\rm BH} = 10^{6.63}\ M_\odot$) on the excess variance versus black hole mass relation presented in Figure 8 of Miniutti et al. (2009), and find that it does follow closely the relation. It should be noted that, J1140+0307, one of the three objects in Miniutti et al. (2009) that are in our sample, is also typical NLS1. As it is generally believed that $M_{\rm BH}$ is the underlying physical parameter that drives the dependence of the X-ray variability, the fact that these NLS1s follow the same excess variance–$M_{\rm BH}$ relation as normal broadline Seyfert 1 galaxies (BLS1s) and quasars tends to validate their $M_{\rm BH}$ estimation. That is to say, the black hole masses of the VNLS1s in our sample are indeed relatively small, i.e., their narrow Balmer linewidth is caused primarily by relatively small $M_{\rm BH}$, rather than by a face-on flattened BLR as claimed in some papers in the literatures.

5. OPTICAL/UV TO X-RAY SPECTRAL INDEX

The broadband spectral energy distribution of AGNs is commonly parameterized by the $\alpha_{\rm ox}$ parameter, $\alpha_{\rm ox} = -0.3838\log[{\rm L}_\nu(2500\ {\rm Å})/{\rm L}_\nu(2\ {\rm keV})]$ (Tananbaum et al. 1979), which is claimed to be correlated with the optical–UV luminosity for Seyferts and quasars (Vignali et al. 2003; Yuan et al. 1998; Strateva et al. 2005). Gallo (2006) reported that the objects in their NLS1 sample, which have systematically broader linewidths than ours, also follow the same relation for BLS1s. Here we investigate this relation for our VNLS1s. The flux density at 2500 Å is calculated from the SDSS u band (effective observed-frame wavelength of 3543 Å) PSF–magnitude adopting the spectral slope of the composite SDSS quasar spectrum ($\alpha_\nu = -0.44$; Vanden Berk et al. 2001). The $\alpha_{\rm ox}$ values of our objects are found to lie in the range from -1.41 to -1.18. We show in Figure 10 the $\alpha_{\rm ox}$ versus 2500 Å monochromatic luminosity relation for our objects, along with the normal NLS1s from the Gallo (2006) sample, as well as the regression relation for normal Seyferts and quasars (Strateva et al. 2005). It shows that the VNLS1s do follow closely the $\alpha_{\rm ox}$–$L_{\rm uv}$ relation defined

[10] Note that the Γ_s values in Grupe et al. (2010) are measured in the 0.2–2 keV band, slightly different from 0.2–2.4 keV adopted here; however, we find from spectral fits that the differences in Γ_s thus caused are negligible for our objects.

[11] For J0107+1408, J1140-0307, and J1357+6525, the X-ray light curves have been presented in Miniutti et al. (2009) and Dewangan et al. (2008); for J1415−0030 it was in Foschini et al. (2004).

[12] Defined as the variance of the light curve in a specific time series after subtracting the contribution expected from measurement errors (e.g., Vaughan et al. 1999).

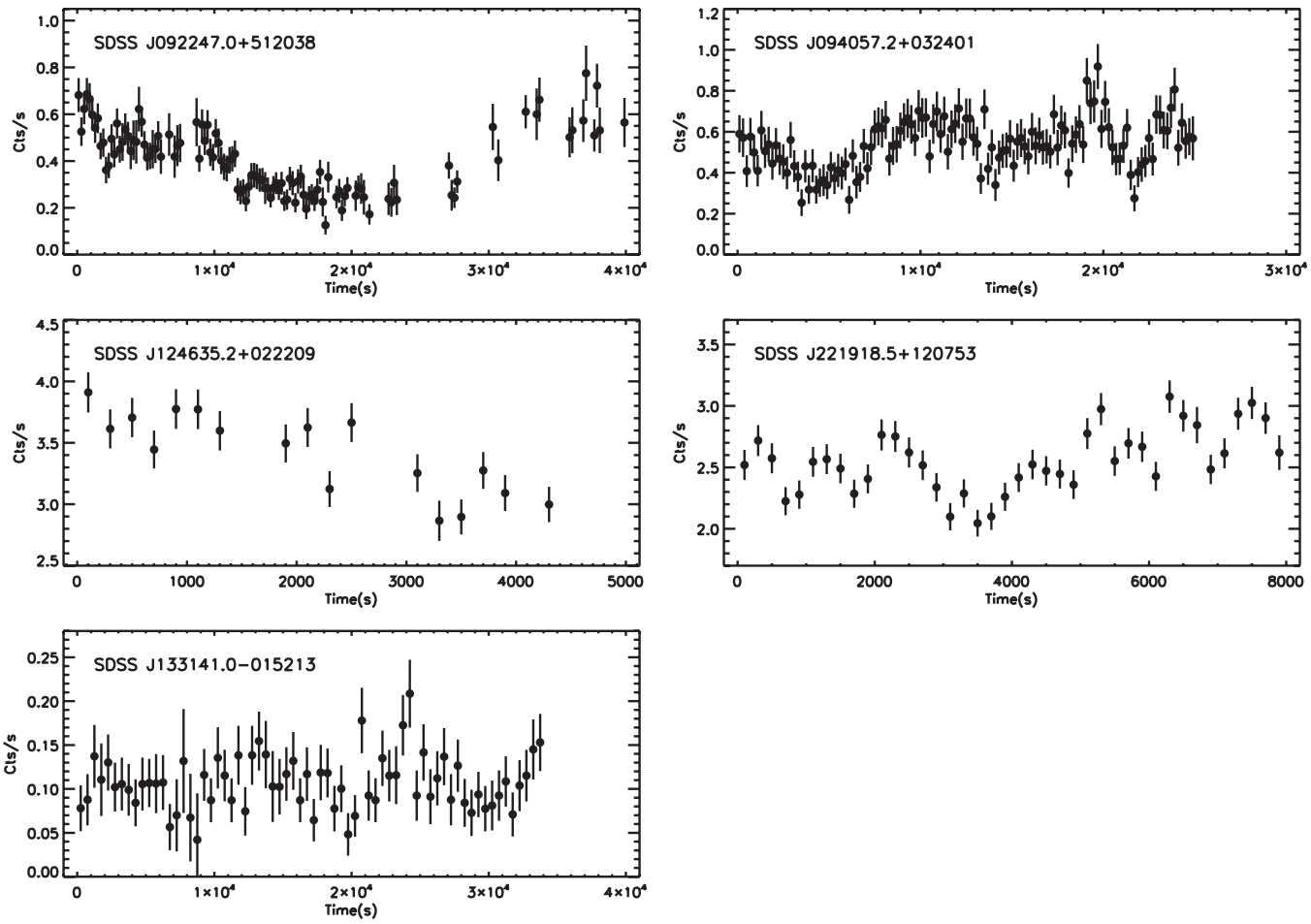

Figure 9. *XMM-Newton* X-ray light curves in the 0.2–10 keV band for five of the VNLS1s in our sample. The time bin size is 200 s, except for SDSS J133141.0−015213 (500 s).

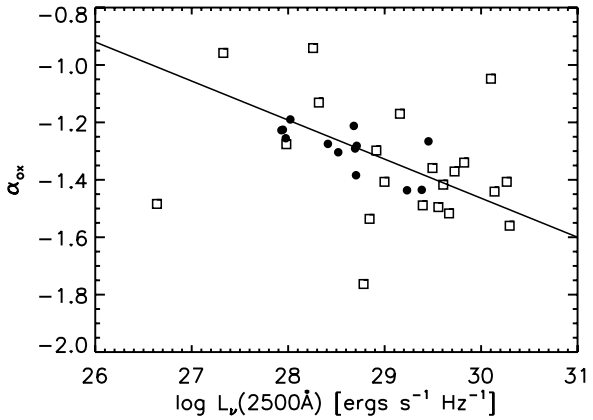

Figure 10. Dependence of α_{ox} on the 2500 Å monochromatic luminosity for the VNLS1s in our sample (filled dots) and the ordinary NLS1s (open squares) in the sample of Gallo (2006). The solid line represents the relation for radio-quiet type 1 AGNs given in Strateva et al. (2005).

by BLS1s, and are consistent with the result for NLS1s with broader linewidths (FWHM $\gtrsim$ 1000 km s^{-1}).

6. DISCUSSION

6.1. Soft X-ray Excess in VNLS1s

The ubiquity of the soft X-ray excess in our VNLS1 sample is interesting, which may have something to do with the generally high $L/L_{\rm Edd}$ in our sample. The reflection model has been found to be a good description of the complexity of the X-ray spectra and spectral variability for several NLS1s (Miniutti & Fabian 2004; Crummy et al. 2006; Ballo et al. 2008; Zoghbi et al. 2008). In some cases the reflection component is found to dominate the observed X-ray band, which can be explained either in terms of a corrugated disk or strong gravitational light bending effects (Fabian et al. 2002). Miniutti et al. (2009) found that this model reproduced well the *XMM-Newton* spectra of several AGNs with $M_{\rm BH} \leqslant 10^6\,M_\odot$, three of which are included in this paper. The spectral fitting for the other objects in our sample also supports this result. The small inner radii of the accretion disk derived argue for fast rotating black holes in most of these VNLS1s, which may be a consequence of their fast accretion process. In a few cases the disk thermal emission is required, which is not unexpected given the relatively high disk temperatures for small $M_{\rm BH}$; this indicates that the disk reflection model is self-consistent.

The Comptonization model successfully explains the soft excess in normal Seyferts (Gierliński & Done 2004) and the spectral variability in RE J1034+396 (Middleton et al. 2009). However, as pointed out by Gierliński & Done (2004), the derived electron temperatures and the optical depth are both found in a small range ($kT_{\rm e} \sim$ 0.1–0.3 keV and $\tau \sim$ 10–20), which is puzzling and requires fine-tuning of the disk parameters. Our result confirms that this is also the case for VNLS1s.

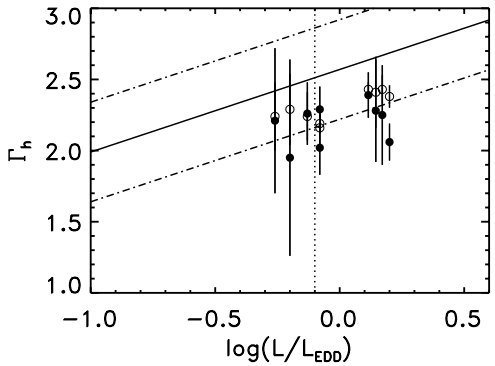

Figure 11. Relationship between the hard X-ray (2–10 keV) photon index and the Eddington ratio for our sample objects. Filled circles represent the results from the fits with a simple power-law model and open circles from a power-law plus disk reflection model. The solid line is the extrapolation of the relation suggested by Risaliti et al. (2009; $M_{\rm BH}$ estimated from Hβ, the same as in our paper) and the dash-dotted line represents the dispersion. The vertical dotted line marks the higher end of the $L/L_{\rm Edd}$ range in the Risaliti's sample.

Although the "p-free" model gives statistically acceptable fitting results in most of the objects, the inferred radii of the innermost disks are unphysically smaller than the gravitational radii. We thus consider the simple "p-free" model to be unfeasible. The smeared absorption model can also reproduce the observed soft X-ray excess to some extent; however, it is disfavored since it results in generally poorer fitting statistics compared to the other models for our sample. Furthermore, the derived velocities are largely unconstrained at the extreme value and the ionization parameters are always found to lie in a narrow range.

6.2. Correlations of Spectral Indices

Our result supports the lack of objects with very steep soft X-ray slopes and FWHM(Hβ) $\lesssim$ 1200 km s^{-1} in the $\Gamma_{\rm s}$–FWHM diagram; those objects may be expected simply based on this well-known EV1 correlation. Here we try to link this relationship with $L/L_{\rm Edd}$, which is believed to be the underlying driver of the EV1 correlations. The soft X-ray spectral slope is primarily determined by two factors: the slope of the underlying (hard X-ray) continuum and the effect of the soft X-ray excess. We examine the effect of the former by comparing the soft and hard band spectral indices of our sample objects and find that they are strongly correlated with each other (a Spearman correlation test probability $P < 10^{-5}$). Thus, we conclude that the soft X-ray slope $\Gamma_{\rm s}$ is largely determined by or traces the underlying continuum slope $\Gamma_{\rm h}$.

Compared to the Γ–FWHM relation, a more significant, and perhaps fundamental, correlation is the $\Gamma_{\rm h}$–$L/L_{\rm Edd}$ correlation that has been detected in the range of $L/L_{\rm Edd} < 1$ (Shemmer et al. 2006; Risaliti et al. 2009). We show in Figure 11 the $\Gamma_{\rm h}$–$L/L_{\rm Edd}$ relation for our VNLS1s whose $\Gamma_{\rm h}$ are available. Also plotted is, for comparison, the regression of Risaliti et al. (2009) for the strongest $\Gamma_{\rm h}$–$L/L_{\rm Edd}$ relation ($M_{\rm BH}$ estimated from Hβ, the same as in our paper) and its extrapolation to the high $L/L_{\rm Edd}$ regime where our sample objects are located. Interestingly, the $\Gamma_{\rm h}$ values of all our VNLS1s fall systematically below the extrapolation of the Risaliti et al.'s relation to high-$L/L_{\rm Edd}$ values. To check whether this flattening might be caused by the enhanced Compton reflection hump—known to exist in Seyfert galaxies and to make the hard X-ray spectrum flatten—in high-$L/L_{\rm Edd}$ objects, we overplot the "underlying" X-ray continuum slope inferred from the above disk reflection model fitting. As can be seen, the "underlying" hard X-ray continua (open circles) are indeed slightly steeper than the "observed" one, but are still systematically flatter than the prediction of the Risaliti et al.'s relation. We thus suggest that, at $L/L_{\rm Edd} \sim 1$ or above, the hard X-ray spectra become flattened than what Risaliti et al.'s relation predicts, at least for the VNLS1s in our sample. Certainly more observations are needed to confirm this trend. If confirmed, this trend in the $\Gamma_{\rm h}$–$L/L_{\rm Edd}$ relation may naturally explain the above observed lack of objects with very steep soft X-ray spectra (i.e., $\Gamma_{\rm s} \gtrsim 3.5$) at the lowest FWHM end.

6.3. Comparison with IMBH AGNs

Three objects in our sample were studied by Miniutti et al. (2009) as AGNs with intermediate mass black holes (IMBHs), a term sometimes used to refer to black holes with $M_{\rm BH} < 10^6\,M_\odot$ in the literature (e.g., Greene & Ho 2004). Since $M_{\rm BH} \propto {\rm FWHM}^2$, most IMBH AGNs must have broad-line widths falling within the conventional criterion of NLS1s ($\lesssim$2000 km s^{-1}), but may not necessarily possess the characteristics of typical NLS1s, i.e., strong Fe II emission, high Eddington ratios, and significant soft X-ray excess (e.g., Greene & Ho 2004). The X-ray properties of IMBH AGN samples have been studied by several authors (Greene & Ho 2007a; Dewangan et al. 2008; Desroches et al. 2009; Miniutti et al. 2009), and a large diversity has been found. For instance, the soft X-ray (0.5–2 keV) photon indices are found to fall into a large range ($\Gamma_{\rm s}$ = 1–2.7; Desroches et al. 2009). The flat X-ray spectral slopes, as well as some other properties, are very similar to those of typical Seyfert galaxies with $M_{\rm BH} = 10^7$–$10^8\,M_\odot$. Some, especially those with low $L/L_{\rm Edd}$, do not show soft X-ray excess (Iwasawa et al. 2000; Dewangan et al. 2008), as in NGC 4395, the prototype of this kind.

We suggest that IMBH AGNs, albeit their small linewidths as for NLS1s, have diverse observed properties, depending on the Eddington ratio. Those accreting at high $L/L_{\rm Edd}$ values are probably more NLS1-like, e.g., the presence of a significant soft X-ray excess, strong FeII, steep $\Gamma_{\rm s}$, such as the three IMBHs in Miniutti et al. (2009) and also included in our sample as VNLS1. On the other hand, there exists a population accreting at low $L/L_{\rm Edd}$, which exhibit properties resembling closely those of classical Seyfert galaxies with more massive $M_{\rm BH}$, in both optical and X-ray (week FeII, relatively flat $\Gamma_{\rm s}$, non-ubiquity of the soft X-ray excess). The observed spectral properties of Seyfert galaxies depend much more strongly on mass accretion rate than on black hole mass. In this regard, the conventional definition of NLS1s may have to be revised. On the other hand, NLS1s and IMBH AGNs show similar timing property. This is not surprising given the postulation that the X-ray variability of AGNs is believed to be largely determined by black hole mass, rather than accretion rate.

7. SUMMARY

NLS1s with very small broadline widths represent the extreme of Seyfert 1 AGNs, which have the largest $L/L_{\rm Edd}/M_{\rm BH}$ ratio among all AGNs known so far. Here we investigated the X-ray properties of a homogeneously selected sample of NLS1s with FWHM(Hβ) $\lesssim$ 1200 km s^{-1}, using the archival *XMM-Newton* data. We note that our sample is not complete in the sense that only those observed with *XMM-Newton* with good spectral S/N are included, which might be biased toward relatively bright objects in X-rays. This should be kept in mind when comparing our results with the others.

No significant Fe Kα emission line is detected, which should be at most weak in such objects. It is found that the soft X-ray excess is ubiquitous in the objects which have the 0.2–10 keV spectra available. The temperatures of this component, when fitted with a blackbody (or disk blackbody) model, all fall within 0.1–0.2 keV, significantly higher than the prediction of the standard disk model. Our result highlights the puzzling independence of the thermal temperature on $M_{\rm BH}$ by extending it to NLS1s with narrower FWHM(Hβ), i.e., smaller $M_{\rm BH}$ and/or higher $L/L_{\rm Edd}$. The failure to ascribe the soft X-ray excess to the Wien tail of the disk blackbody emission in these VNLS1s (with similar $M_{\rm BH}$ and $L/L_{\rm Edd}$ values to RX J1633+4718, though) highlights the question as to why RX J1633+4718 is so unique (see Yuan et al. 2010 for a brief discussion). A range of viable models, including Comptonization, disk reflection, smeared absorption, and the p-free model, were used to fit the soft X-ray excess. In general, the disk reflection and Comptonization models tend to give the best fits. The relative strength of the soft X-ray excess appears to be independent of FWHM(Hβ) over a large range, indicating that the excess component is not particularly strong in these VNLS1s compared to PG quasars with much broader linewidth.

The soft X-ray spectra in 0.2–2.4 keV have a mean photon index of $\Gamma_{\rm s}$=$2.83^{+0.19}_{-0.20}$ with a large intrinsic scatter ($\sigma = 0.31^{+0.20}_{-0.10}$), while the 2–10 keV spectra have a mean $\Gamma_{\rm h}$ of $2.19^{+0.19}_{-0.18}$ with a small intrinsic scatter consistent with zero. Thus, VNLS1s have the spectral slopes in both bands no steeper than "normal" NLS1s with broader linewidth. There is little or no intrinsic X-ray absorption in most of these VNLS1s, indicating that the flattening of the $\Gamma_{\rm s}$–FWHM anti-correlation below FWHM $\sim$1200 km s^{-1}, as suggested in Zhou et al. (2006; using a much larger sample but with $\Gamma_{\rm s}$ estimated from hardness ratios), is not caused by absorption but most likely intrinsic. Although this trend is not statistically significant when combining our current sample with the *Swift* sample of Grupe et al. (2010), both with $\Gamma_{\rm s}$ derived from spectral fitting, there appears to be a lack of AGNs with both very narrow FWHM(Hβ) ($\lesssim$1000 km s^{-1}) and very steep soft X-ray spectra (i.e., $\Gamma_{\rm s} \gtrsim 3.5$). Furthermore, there is a tentative hint that the hard X-ray slopes $\Gamma_{\rm h}$ of our objects fall systematically below the extrapolation of the suggested $\Gamma_{\rm h}$–$L/L_{\rm Edd}$ correlation (Risaliti et al. 2009) to high $L/L_{\rm Edd}$ values. We argue that these two trends, if confirmed, might in fact be driven by the same underlying physical process. Similar to other "normal" NLS1s, these VNLS1s also follow the same $\alpha_{\rm ox}$–$L_{\rm opt}$ relation as for normal Seyferts and quasars.

All of the sample objects show rapid variability in X-rays, with two-fold timescales of 1–2 hr. The short variability timescales and the conformance with the variance excess–black hole mass relation for normal Seyferts tend to suggest that the black hole masses in these VNLS1s are likely truly small, as commonly thought, and the present $M_{\rm BH}$ estimators based on the linewidth–luminosity scaling relation are applicable to NLS1s.

We thank the referee for helpful comments and suggestions, which helped to improve the paper significantly. Y.A. is grateful to Stefanie Komossa for tutorials on the X-ray data analysis and discussions on this work, and her kind hospitality during the visit at MPE. Y.A. is grateful for the support by the MPG–CAS Joint Doctoral Promotion Programme and the hospitality of MPE, where part of the research was carried out. This work is supported by NSFC grants 10533050, 11033007, and the National Basic Research Program of (973 Program) 2009CB824800, 2007CB815405. This research is based on observations obtained with *XMM-Newton*, an ESA science mission with instruments and contributions directly funded by ESA Member States and NASA. Funding for the SDSS and SDSS-II was provided by the Alfred P. Sloan Foundation, the Participating Institutions, the National Science Foundation, the US Department of Energy, the National Aeronautics and Space Administration, the Japanese Monbukagakusho, the Max Planck Society, and the Higher Education Funding Council for England. The SDSS Web site is http://www.sdss.org/.

APPENDIX

COMPARISONS WITH PREVIOUS RESULTS FOR INDIVIDUAL OBJECTS

For six objects in our sample, the *XMM-Newton* data have been presented previously. Here we compare our results with those in the literature.

J0107+1408, J140+0307, J1357+6525. These three objects were studied as IMBH AGNs by Miniutti et al. (2009) and Dewangan et al. (2008). For the model fits with blackbody, ionized disk reflection, and smeared absorption, our results are consistent with the previous ones except that the disk ionization parameters of ours are somewhat higher than those in Miniutti et al. (2009). In addition, we fit the spectra with the Comptonization and "p-free" model, which was not considered in the previous papers.

J1246+0222. The fitting results for the soft X-ray excess component are consistent with those presented in the literature (Porquet et al. 2004; Crummy et al. 2006; Middleton et al. 2007). However, in the simple power-law fitting we find a soft X-ray photon index of 2.97 $\pm$ 0.06 while Porquet et al. (2004) gave the value of 3.72 $\pm$ 0.09.

J1415−0030. The *XMM-Newton* data were presented previously by Foschini et al. (2004), who fitted the spectrum with the simple power-law plus blackbody model only, and gave a somewhat flatter photon index (1.8 $\pm$ 0.2) than ours ($2.42^{+0.12}_{-0.20}$). We find that there is an edge-like feature around 0.6 keV for J1415−0030.

J2219+1207. The spectrum was fitted with a power-law plus blackbody model by Gallo et al. (2006), giving a result consistent with ours. The authors also noted the broad excess emission feature around 5.8 keV, which was fitted with a broad emission line; while in our work the disk reflection model can reproduce this feature well.

REFERENCES

Abdo, A. A., et al. 2009, ApJ, 699, 976
Abramowicz, M. A., Czerny, B., Lasota, J. P., & Szuszkiewicz, E. 1988, ApJ, 332, 646
Arnaud, K. A. 1996, in ASP Conf. Ser. 101, Astronomical Data Analysis Software and Systems V, ed. G. Jacoby & J. Barnes (San Francisco, CA: ASP), 17
Ballo, L., Giustini, M., Schartel, N., Cappi, M., Jiménez-Bailón, E., Piconcelli, E., Santos-Lleó, M., & Vignali, C. 2008, A&A, 483, 137
Bentz, M. C., Peterson, B. M., Pogge, R. W., Vestergaard, M., & Onken, C. A. 2006, ApJ, 644, 133
Bianchi, S., Guainazzi, M., Matt, G., Fonseca Bonilla, N., & Ponti, G. 2009, A&A, 495, 421
Boller, T., Brandt, W. N., & Fink, H. 1996, A&A, 305, 53
Boroson, T. A., & Green, R. F. 1992, ApJS, 80, 109
Crummy, J., Fabian, A. C., Gallo, L., & Ross, R. R. 2006, MNRAS, 365, 1067
Czerny, B., & Elvis, M. 1987, ApJ, 321, 305
Czerny, B., Nikołajuk, M., Różańska, A., Dumont, A.-M., Loska, Z., & Życki, P. T. 2003, A&A, 412, 317
Desroches, L.-B., Greene, J. E., & Ho, L. C. 2009, ApJ, 698, 1515

Dewangan, G. C., Mathur, S., Griffiths, R. E., & Rao, A. R. 2008, ApJ, 689, 762
Elvis, M., et al. 1994, ApJS, 95, 1
Fabian, A. C., Ballantyne, D. R., Merloni, A., Vaughan, S., Iwasawa, K., & Boller, Th. 2002, MNRAS, 331, 35
Foschini, L., et al. 2004, A&A, 428, 51
Gallo, L. C. 2006, MNRAS, 368, 479
Gallo, L. C., Lehmann, I., Pietsch, W., Boller, Th., Brinkmann, W., Friedrich, P., & Grupe, D. 2006, MNRAS, 365, 688
Gierliński, M., & Done, C. 2004, MNRAS, 349, 7
Gierliński, M., Middleton, M., Ward, M., & Done, C. 2008, Nature, 445, 369
Goodrich, R. W. 1989, ApJ, 342, 224
Greene, J. E., & Ho, L. C. 2004, ApJ, 610, 722
Greene, J. E., & Ho, L. C. 2007a, ApJ, 656, 84
Greene, J. E., & Ho, L. C. 2007b, ApJ, 670, 92
Grupe, D. 2004, AJ, 127, 1799
Grupe, D., Komossa, S., Leighly, K. M., & Page, K. L. 2010, ApJS, 187, 64G
Guainazzi, M. 2010, XMM-EPIC Status of Calibration and Data Analysis, XMM-SOC-CAL-TN-0018
Iwasawa, K., Fabian, A. C., Almaini, O., Lira, P., Lawrence, A., Hayashida, K., & Inoue, H. 2000, MNRAS, 318, 879
Kaspi, S., Maoz, D., Netzer, H., Peterson, B. M., Vestergaard, M., & Jannuzi, B. T. 2005, ApJ, 629, 61
Kawaguchi, T. 2003, ApJ, 593, 69
Komossa, S. 2008, RevMexAA, 32, 86
Laor, A. 1991, ApJ, 376, 90
Laor, A. 2000, New Astron. Rev., 44, 503
Leighly, K. M. 1999, ApJS, 125, 297
Lu, Y.-J., & Yu, Q.-J. 2001, ApJ, 561, 660
Maccacaro, T., Gioia, I. M., Wolter, A., Zamorani, G., & Stocke, J. T. 1988, ApJ, 326, 680
McHardy, I. M., Koerding, E., Knigge, C., Uttley, P., & Fender, R. P. 2006, Nature, 444, 730
Middleton, M., Done, C., & Gierliński, M. 2007, MNRAS, 381, 1426
Middleton, M., Done, C., Ward, M., Gierliński, M., & Schurch, N. 2009, MNRAS, 394, 250
Mineshige, S., Kawaguchi, T., Takeuchi, M., & Hayashida, K. 2000, PASJ, 52, 499
Miniutti, G., & Fabian, A. C. 2004, MNRAS, 349, 1435
Miniutti, G., Ponti, G., Greene, J. E., Ho, L. C., Fabian, A. C., & Iwasawa, K. 2009, MNRAS, 394, 443
O'Neill, P. M., Nandra, K., Papadakis, I. E., & Turner, T. J. 2005, MNRAS, 358, 1405
Onken, C. A., & Peterson, B. M. 2002, ApJ, 572, 746
Osterbrock, D. E., & Pogge, R. W. 1985, ApJ, 297, 166
Page, K. L., O'Brien, P. T., Reeves, J. N., & Turner, M. J. L. 2004, MNRAS, 347, 316
Papadakis, I. E. 2004, MNRAS, 348, 207
Peterson, B. M. 1997, An Introduction to Active Galactic Nuclei (Cambridge: Cambridge Univ. Press)
Peterson, B. M., & Wandel, A. 2000, ApJ, 540, 13
Peterson, B. M., et al. 2000, ApJ, 542, 161
Piconcelli, E., Jimenez-Bailón, E., Guainazzi, M., Schartel, N., Rodríguez-Pascual, P. M., & Santos-Lleó, M. 2005, A&A, 432, 15
Porquet, D., Reeves, J. N., O'Brien, P., & Brinkmann, W. 2004, A&A, 422, 85
Pounds, K. A., Done, C., & Osborne, J. P. 1995, MNRAS, 277, 5
Risaliti, G., Young, M., & Elvis, M. 2009, ApJ, 700, 6
Ross, R. R., & Fabian, A. C. 1993, MNRAS, 261, 74
Ross, R. R., & Fabian, A. C. 2005, MNRAS, 358, 211
Shemmer, O., Brandt, W. N., Netzer, H., Maiolino, R., & Kaspi, S. 2006, ApJ, 646, 29
Shimura, T., & Takahara, F. 1993, ApJ, 419, 78
Strateva, I. V., Brandt, W. N., Schneider, D. P., Vanden Berk, D. G., & Vignali, C. 2005, AJ, 130, 387
Sulentic, J. W., Zwitter, T., Marziani, P., & Dultzin-Hacyan, D. 2000, ApJ, 536, L5
Tananbaum, H., et al. 1979, ApJ, 234, L9
Titarchuk, L. 1994, ApJ, 434, 570
Vanden Berk, D. E., et al. 2001, AJ, 122, 549
Vaughan, S., Reeves, J., Warwick, R., & Edelson, R. 1999, MNRAS, 309, 113
Véron-Cetty, M.-P., Véron, P., & Gonçalves, A. C. 2001, A&A, 372, 730
Vignali, C., Brandt, W. N., & Schneider, D. P. 2003, AJ, 125, 433
Wandel, A., & Petrosian, V. 1988, ApJ, 329, 11
Wang, T., Brinkmann, W., & Bergeron, J. 1996, A&A, 309, 81
Watson, M. 2007, Astron. Geophys., 48, 30
Yuan, W., Brinkmann, W., Siebert, J., & Voges, W. 1998, A&A, 330, 108
Yuan, W., Liu, B. F., Zhou, H., & Wang, T. G. 2010, ApJ, 723, 508
Yuan, W., Zhou, H. Y., Komossa, S., Dong, X. B., Wang, T. G., Lu, H. L., & Bai, J. M. 2008, ApJ, 685, 801
Zhou, H.-Y., Wang, T.-G., Yuan, W., Lu, H.-L., Dong, X.-B., Wang, J.-X., & Lu, Y.-J. 2006, ApJS, 166, 128
Zhou, H.-Y., et al. 2007, ApJ, 658, 13
Zoghbi, A., Fabian, A. C., & Gallo, L. C. 2008, MNRAS, 391, 2003